JLR RESEARCH ARTICLE

ω-*O*-Acylceramides but not ω-hydroxy ceramides are required for healthy lamellar phase architecture of skin barrier lipids

Lukáš Opálka[1], Jason M. Meyer[2], Veronika Ondrejčeková[1], Linda Svatošová[1], Franz P. W. Radner[3], and Kateřina Vávrová[1]*

[1]Charles University, Faculty of Pharmacy in Hradec Králové, Hradec Králové, Czech Republic; [2]Department of Dermatology, Vanderbilt University Medical Center, Nashville, TN, USA; [3]Institute of Molecular Biosciences, University of Graz, Graz, Austria

Abstract Epidermal omega-*O*-acylceramides (ω-*O*-acylCers) are essential components of a competent skin barrier. These unusual sphingolipids with ultralong *N*-acyl chains contain linoleic acid esterified to the terminal hydroxyl of the *N*-acyl, the formation of which requires the transacylase activity of patatin-like phospholipase domain containing 1 (PNPLA1). In ichthyosis with dysfunctional PNPLA1, ω-*O*-acylCer levels are significantly decreased, and ω-hydroxylated Cers (ω-OHCers) accumulate. Here, we explore the role of the linoleate moiety in ω-*O*-acylCers in the assembly of the skin lipid barrier. Ultrastructural studies of skin samples from neonatal *Pnpla1*$^{+/+}$ and *Pnpla1*$^{-/-}$ mice showed that the linoleate moiety in ω-*O*-acylCers is essential for lamellar pairing in lamellar bodies, as well as for stratum corneum lipid assembly into the long periodicity lamellar phase. To further study the molecular details of ω-*O*-acylCer deficiency on skin barrier lipid assembly, we built in vitro lipid models composed of major stratum corneum lipid subclasses containing either ω-*O*-acylCer (healthy skin model), ω-OHCer (*Pnpla1*$^{-/-}$ model), or combination of the two. X-ray diffraction, infrared spectroscopy, and permeability studies indicated that ω-OHCers could not substitute for ω-*O*-acylCers, although in favorable conditions, they form a medium lamellar phase with a 10.8 nm-repeat distance and permeability barrier properties similar to long periodicity lamellar phase. In the absence of ω-*O*-acylCers, skin lipids were prone to separation into two phases with diminished barrier properties. The models combining ω-OHCers with ω-*O*-acylCers indicated that accumulation of ω-OHCers does not prevent ω-*O*-acylCer-driven lamellar stacking. These data suggest that ω-*O*-acylCer supplementation may be a viable therapeutic option in patients with PNPLA1 deficiency.

Supplementary key words Skin • lipids • ceramides • sphingolipids • acylceramides • barrier function • stratum corneum • model membranes • linoleic acid • PNPLA1 deficiency

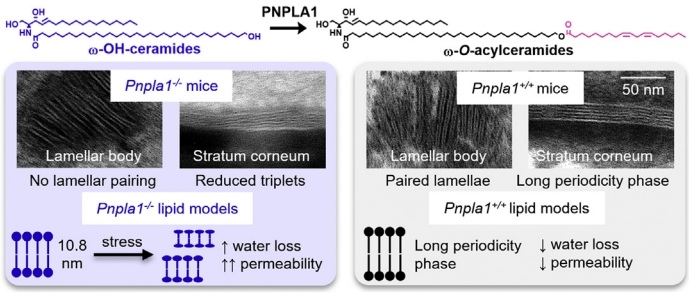

The outermost skin layer, the stratum corneum, protects the mammalian body from potentially harmful environmental substances and excessive water loss (1). The stratum corneum comprises terminally differentiated cells, known as corneocytes, surrounded by extracellular lipid lamellae, which are critical for the permeability barrier homeostasis. The stratum corneum lipids consist of an approximately 1:1:1 molar mixture of ceramides (Cers), free fatty acids (FFAs), and cholesterol (Chol), with minor components such as cholesteryl sulfate (CholS) (2). Skin Cers are an extremely heterogeneous group comprising at least 16 subclasses (supplemental Fig. S1) (3), including non-hydroxylated and α-hydroxylated very long chain Cers and epidermal-specific ω-*O*-acylceramides (ω-*O*-acylCers, **Fig. 1**).

The ω-*O*-acylCers (such as *N*-(ω-*O*-linoleoyloxy)acyl sphingosine, Cer EOS according to the nomenclature system by Motta *et al.* (4)) have linoleic acid ester-bound at the ω-end of their *N*-acyl chains, typically ultralong (up to 36 carbon atoms) (5–8), and their synthesis requires several specific steps (9). These lipids comprise around 10 weight % (7 mol%) of the extractable stratum corneum Cers (3, 6, 10, 11). The ω-*O*-acylCers are essential for the typical stratum corneum multilamellar lipid assemblies with approximately 11–13 nm repeat distance, the long periodicity lamellar phase (LPP) (12–14). Due to its two *cis*-

*For correspondence: Kateřina Vávrová, katerina.vavrova@faf.cuni.cz.

 https://doi.org/10.1016/j.jlr.2022.100226

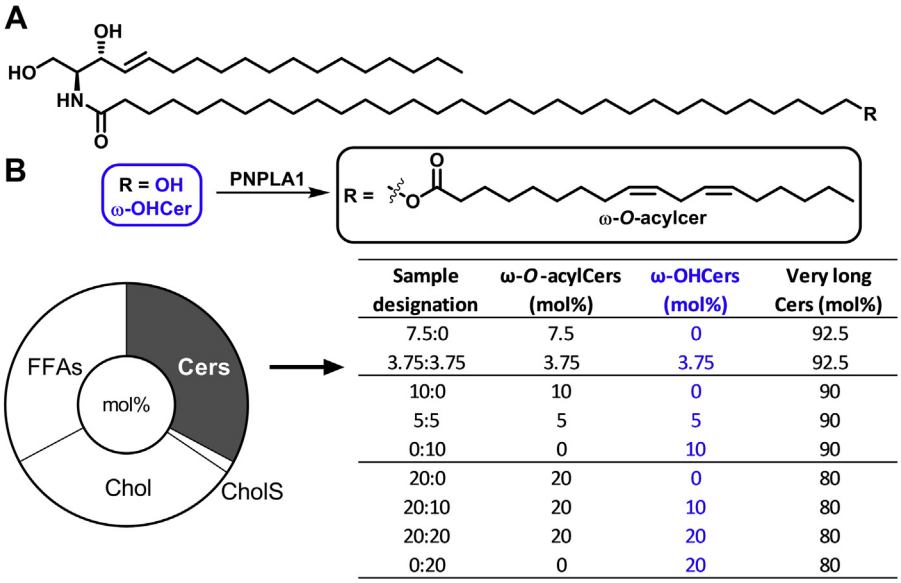

Sample designation	ω-*O*-acylCers (mol%)	ω-OHCers (mol%)	Very long Cers (mol%)
7.5:0	7.5	0	92.5
3.75:3.75	3.75	3.75	92.5
10:0	10	0	90
5:5	5	5	90
0:10	0	10	90
20:0	20	0	80
20:10	20	10	80
20:20	20	20	80
0:20	0	20	80

Fig. 1. Molecular structures of the studied ω-OHCers and ω-*O*-acylCers (A), the model compositions in mol% (B; donut chart), and the compositions of the ceramide fractions in the models in mol% (B; table). ω-O-acylCers, omega-O-acylceramides; ω-OHCers, ω-hydroxylated Cers.

double bonds, ω-esterified linoleate is fluid at skin temperature (15) in contrast to the *N*-acyl chains, which are primarily rigid and tightly packed (16). The linoleate moiety in ω-*O*-acyl(glucosyl)Cers is fundamental for attaching to corneocyte proteins to form the corneocyte lipid envelope (CLE) (17–19).

The CLE and the LPP arrangement of the stratum corneum lipids are vital for permeability barrier function (20, 21). The complete ω-*O*-acylCer deficit is lethal to neonatal mice (22), while diminished ω-*O*-acylCer levels in humans contribute to disturbed epidermal homeostasis in skin disorders (23) such as atopic dermatitis (10, 21, 24, 25), psoriasis (4), or ichthyoses (26). In particular, several autosomal recessive congenital ichthyoses have altered ω-*O*-acylCer metabolism (27, 28). For example, the linoleate attachment to the ω-hydroxyl group on the Cer ultra-long acyl chain requires transacylase activity of patatin-like phospholipase domain containing 1 (PNPLA1) (29). Dysfunctional *Pnpla1* gene in mice led to significantly decreased ω-*O*-acylCer levels and an accumulation of ω-hydroxylated Cers (ω-OHCers), diminished CLE, and impaired lamellar organization of the stratum corneum extracellular lipids (30–33). Such ω-OHCers, which lack the linoleate moiety are present only in small amounts in healthy skin (6).

Here, we explore the role of the linoleate moiety in ω-*O*-acylCers in the skin barrier lipid assembly. First, electron microscopy was used to examine the effect of *Pnpla1* expression on epidermal lamellar lipid organization in vivo. Next, we built in vitro multilamellar lipid models composed of major stratum corneum lipid subclasses, either with ω-*O*-acylCer (healthy skin model) or with ω-OHCer (*Pnpla1*$^{-/-}$ model) or their combinations (model of partial PNPLA1 dysfunction and models of PNPLA1-deficient skin treated with ω-*O*-acylCer; Fig. 1). The ω-*O*-acylCers and ω-OHCers comprised sphingosine, dihydrosphingosine, and phytosphingosine as their sphingoid backbones, that is, they were mixtures of EOS/EOdS/EOP and OS/OdS/OP, respectively. Selected lipid models were stressed by assembling them at a higher temperature and reduced hydration. The lamellar organization of these models using various ω-*O*-acylCer/ω-OHCer concentrations was assessed by X-ray diffraction (XRD). Selected models were further examined by Fourier-transform infrared spectroscopy (FTIR) for their lipid chain order, packing, and transitions. Permeabilities of the lipid models, sandwiched in Franz cells, were probed by water loss measurements and two permeants.

MATERIALS AND METHODS

Chemicals

ω-O-acylCers [Cer EOS (d18:1/h32:0/18:2), Cer EOP (t18:0/h32:0/18:2), and Cer EOdS (d18:0/h32:0/18:2)] were prepared as described previously (34). ω-OHCers [Cer OS (d18:1/h32:0), Cer OP (t18:0/h32:0), and Cer OdS (d18:0/h32:0)] were prepared by a modified procedure described in Opálka *et al.* (34) that will be published elsewhere. Cer AdS (d18:0/h24:0) was prepared according to Kováčik *et al.* (35) Cer NS (d18:1/24:0), Cer NP (t18:0/24:0), Cer AS (d18:1/h24:0), Cer AP (t18:0/h24:0), and Cer NdS (d18:0/24:0) were purchased from Avanti Polar Lipids. FFAs (lignoceric, behenic, arachidic, stearic, and palmitic acids), Chol, CholS, theophylline (TH), indomethacin (IND), gentamicin sulfate, propylene glycol, buffer components, and solvents were purchased from Merck. All solvents used were of analytical or HPLC grade. Water was purified using a Milli-Q system (Merck Millipore).

Mice and electron microscopy

Pnpla1$^{+/+}$ and *Pnpla1*$^{-/-}$ skin samples were acquired during a previously published study from neonatal mice, in which loss

of *Pnpla1* expression was confirmed (31). All mouse procedures were approved by medical ethics committees at the University of Graz and the Austrian Federal Ministry of Science, Research and Economy. No new mouse procedures were performed as part of the present study. Skin samples were minced into fragments < 0.5 mm^3, prefixed in half-strength Karnovsky's fixative, rinsed three times in 0.1 mol/L cacodylate buffer, followed by postfixation in ruthenium tetroxide (Polysciences). Samples were then embedded in epoxy-Epon (Hexion) and processed for electron microscopy (36). Imaging was done on thin sections using a JEOL 100CX electron microscope at 60 V with a Gatan Bioscan camera (model 792). Images presented in **Fig. 2** represent the entire samples from all three mice within the respective group. The LPP was identified in electron microscope images using the DigitalMicrograph version 3.10.0 (Gatan Inc.) and its length was determined using the density profile tool, while LPP abundance was quantified as percentage of lamellae that were part of an LPP out of the total number of lamellae captured in each image slice.

Preparation of stratum corneum lipid models

The lipid models were prepared from Cers, FFAs, Chol, and CholS as follows (Fig. 1). The Cer fraction consisted of very long Cers NS, NP, NdS, AS, AP, and AdS (in an 8.3:25.3:9.1:26.0:29.8:1.4 M ratio) mixed in different ratios with ω-*O*-acylCers or ω-OHCers (composed of Cers EOS/EOP/EOdS or OS/OP/OdS, respectively, in 78.0:16.4:5.6 M ratios, Fig. 1 and supplemental Table S1). Due to the unavailability of Cers based on 6-hydroxysphingosine, these Cers were (proportionally) substituted with the available Cer subclasses to maintain the same level of hydroxylation as follows: Cer AS was used in place of Cer NH, and Cer AP was used in place of Cer AH. Cer EOH (and Cer OH) were proportionally substituted with Cers EOS (OS), EOdS (OdS), and EOP (OP) in the mixtures. FFAs of even chain lengths (1.3 mol% palmitic, 3.3% stearic, 6.9% arachidic, 47.1% behenic, and 41.4% lignoceric acid) were mixed to approximate their proportions in the healthy human stratum corneum (37, 38).

The lipids were dissolved in $CHCl_3$/MeOH 2:1 (v/v), mixed as shown in Fig. 1, and dried in a vacuum. Then, 1.35 mg of the lipid mixture (per sample) was dissolved in 400 µl of hexane/96% ethanol 2:1 (v/v) and sprayed using a stream of nitrogen as a carrier gas and a Linomat V (Camag) with additional y-axis movement (37) on either a cover glass (22 × 22 mm) for XRD or Nuclepore polycarbonate filters (15 nm pore size, Whatman) for the permeability experiments. The sprayed area was 1 cm^2, and the lipid solution flow rate was 10.2 µl/min. Thus, the films contained 1.35 mg/cm^2 lipid, roughly 10-fold more than in the stratum corneum, partly compensating for the lack of tortuosity in such models. The prepared lipid films were heated above their phase transition temperatures, either at 90°C (at ambient humidity) or 70°C (at 100% relative humidity) for 10 min, and then slowly (overnight) cooled to 32°C. The membrane thickness was approximately 11 µm (39). Before the experiments, the lipids were equilibrated at 32°C and 40%–50% humidity for 24 h (39, 40). The homogeneous lipid distribution was determined by high-performance thin-layer chromatography after the $CHCl_3$/MeOH (2:1 v/v) extraction of the membrane center and periphery (41).

X-ray diffraction

The XRD of the studied lipid membranes was performed using an X'Pert PRO θ – θ powder diffractometer (PANalytical B.V., Almelo) with parafocusing Bragg-Brentano geometry using CoKα radiation (λ = 1.7903 Å, U = 35 kV, I = 40 mA). X-ray focus, type: line, length: 12 mm, width: 0.4 mm, take-off angle: 6°. Incident beam path, soller slit opening: 0.04 rad, beam mask width: 15 mm, automatic programmable divergence slit, irradiated length: 20 mm. Diffracted beam path, fixed anti-scatter slit height: 6.6 mm, soller slit opening: 0.04 rad, and nickel filter thickness: 0.02 mm. Beam knife is used at a fixed height. The samples were mounted in modified sample holders (with an inner diameter of 32 mm, for filters or solid samples with a diameter of 30–32 mm, a maximum thickness of 5.8 mm) over the angular range of 0.6–30° (2 θ). The data were scanned with the ultrafast linear position-sensitive (1D) detector X'Celerator

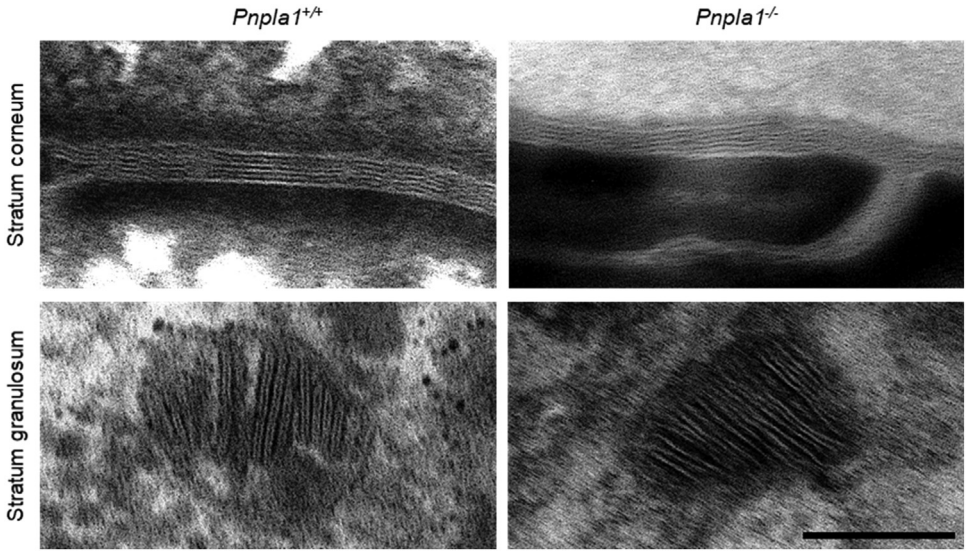

Fig. 2. Ultrastructure of lamellar lipids in *Pnpla1*$^{+/+}$ and *Pnpla1*$^{-/-}$ epidermis. Images show representative lamellar bodies in the stratum granulosum and mature lipid lamellae in the stratum corneum of the indicated mice. Scale bar = 100 nm. These images have been reused in the Graphical abstract.

with a step size of 0.0167° (2 θ) and counting time of 20.32 s/step at room temperature. The data were evaluated using X'Pert Data Viewer (PANalytical B.V., Almelo). The XRD diffractograms show the scattered intensity as a function of the scattering vector q [nm^{-1}], which is proportional to the scattering angle 2 θ according to the following equation: $q = 4\pi \sin\theta/\lambda$ ($\lambda = 0.17903$ nm is the wavelength of the X-rays). No correction factors were applied to the diffraction patterns. The repeat distance d [nm] characterized the regular spacing of parallel lipid layers arranged on a one-dimensional lattice and was obtained from a slope "a" of a linear regression fit of the dependence $qn = a \times n + k$ according to the equation $d = 2\pi/a$. The peaks were assigned to a specific lamellar phase only when $R^2 \geq 0.9998$. This lipid arrangement is called a lamellar phase (L). The diffractograms of the lamellar phases exhibit a set of Bragg reflections, whose reciprocal spacings are in the characteristic ratios of $Qn = 2\pi n/d$ (reflection's order number n = 1, 2, 3…).

Water loss and permeability of the lipid models

Lipid membranes on polycarbonate filters (n = 7 for each sample type) were fixed in homemade Teflon holders with a 0.5 cm^2 circular opening. The holders were mounted in Franz diffusion cells (glass, custom-made, supplemental Fig. S2) with the lipid layer facing the donor compartment. The volume of the individual acceptor parts was 6.8 ± 0.2 ml (the precise volume was measured per cell and included in the calculations). Acceptor compartment of each Franz diffusion cell was filled with PBS buffer at pH 7.4 with 50 mg/ml of gentamicin sulfate and equilibrated at 32°C for 12 h. The lipid film integrity was checked by electrical impedance (all values were higher than 80 kΩ × cm^2) (14, 40, 42).

For the water loss measurement, the donor part of the cell was temporarily removed, and the probe of the Aquaflux AF200 instrument (Biox) was tightly placed on top of the Teflon membrane holder to avoid vapor leakage. The effective measured area was 0.5 cm^2, the measurement time was set to 90 s (or until the steady-state was reached), and the value was recorded in grams per hour per meter squared. The measurements were carried out at 24 ± 1°C ambient temperature and 40%–50% air humidity (conditions for the Aquaflux probe), whereas the temperature of the acceptor phase remained at 32 ± 0.5°C.

Next, 100 µl of a model permeant suspension (5% TH or 2% IND in 60% propylene glycol) was applied directly on top of the lipid membrane in the Franz cell donor compartment. The acceptor phase samples (300 µl) were collected every 2 h for 10 h and replaced with fresh PBS. The cumulative amounts of TH and IND permeated through the lipid models corrected for the PBS replacement were plotted against time. The typical lag times were below 2 h; thus, a 10 h experiment duration was sufficient to reach the steady state. The flux values were calculated as the slopes of the linear part of the permeation profile. The polycarbonate membrane did not affect the permeability, and propylene glycol did not extract any lipids from the membrane, which was demonstrated using high-performance thin-layer chromatography (41).

HPLC

TH or IND in the acceptor phase samples were analyzed using isocratic reverse-phase HPLC on a Shimadzu Prominence instrument (Shimadzu) with "Shimadzu LCsolution Version 1.22" software using a LiChroCART 250-4 column (LiChrospher 100 RP-18, 5 µm particle size, Merck) using validated methods (14, 40, 43). TH separation was achieved using 4:6 MeOH/0.1 M NaH_2PO_4 (v/v) at a 1.2 ml/min flow rate. The column was maintained at 35°C. TH was detected at 272 nm; its retention time was 3.2 ± 0.1 min. For IND, 90:60:5 acetonitrile/water/acetic acid mobile phase was used at 2 ml/min flow rate, and the column was maintained at 40°C. IND was detected at 260 nm and its retention time was 3.1 ± 0.1 min.

Fourier-transform infrared spectroscopy

Selected lipid membranes were measured on a Nicolet 6700 spectrometer (Thermo Scientific) equipped with a single reflection MIRacle ATR ZnSe crystal (PIKE Technologies). The spectra were generated by the coaddition of 256 scans recorded at a 2 cm^{-1} resolution, with a clamping mechanism ensuring constant pressure. Using a temperature control module (PIKE Technologies), the spectra were recorded between 28 and 100°C in 2°C steps (the stabilization time between steps was 6 min). The analysis was performed using Bruker OPUS software. The exact peak positions were determined from the second derivative spectra.

Data treatment

Two samples were compared using Student's t test, three or more samples using one-way ANOVA with Dunnett's post hoc test; $P < 0.05$ was considered significant.

RESULTS

Loss of ω-*O*-acylCer linoleate moiety in *Pnpla1*$^{-/-}$ mice disturbs the lipid lamellae pairing in lamellar bodies and the LPP pattern of the stratum corneum lipids

Lamellar lipid organization in *Pnpla1*$^{+/+}$ epidermis (Fig. 2) was characterized by paired lamellae in lamellar bodies and triplet-grouped lamellae (LPP, with repeat distance 11.5 ± 1.0 nm, mean ± SD, n = 73 determinations) in the stratum corneum, as previously reported (44). In contrast, no lamella pairing was observed in *Pnpla1*$^{-/-}$ lamellar bodies, and the percentage of stratum corneum lamellae that were contained within triplet groupings (LPP with repeat distance 10.1 ± 1.1 nm, mean ± SD, n = 8 determinations) was significantly reduced from 85 ± 26% to 15 ± 35% ($P<0.001$) so that most lamellae were not part of any higher-order lamellar organization.

Loss of ω-*O*-acylCer linoleate moiety in the in vitro stratum corneum lipid models disturbs the LPP arrangement rendering the lipids sensitive to external conditions

Next, several in vitro lipid models were constructed to capture the stratum corneum lipid arrangement changes upon the loss of the linoleate moiety in ω-*O*-acylCers. Synthetic lipids instead of natural extracts were used for these models to precisely control their composition, particularly replacing the ω-*O*-acylCers with ω-OHCers while maintaining the other lipids unaffected. The lipids were annealed at 70°C and 100% relative humidity unless indicated otherwise. The major

limitation of this approach is the lack of in vitro CLE models, which restricts our methods to mimicking the free stratum corneum lipids. As the CLE is virtually absent in *Pnpla1*$^{-/-}$ mice, this drawback disappears, and the ω-OHCer model reasonably mimics the bulk stratum corneum lipids in those mice.

This point of absent CLE in the in vitro lipid models must also be considered when selecting the ω-*O*-acylCer concentration. An ω-*O*-acylCer concentration of approximately 7 mol% was reported in extracted human stratum corneum lipids (3, 6, 10, 11). However, the amount of ultralong chain Cers contributing to the LPP in vivo is higher because the broad electron-lucent band from the CLE is rich in such lipids (despite being immobilized on the cell surface). We addressed this problem by using two sets of models: one with ≤10 and another with 20 mol% ω-*O*-acylCers within the Cer fraction.

First, we examined the lipid mixtures with ω-*O*-acylCers, which approximate the healthy skin lipids, using XRD to establish their lamellar arrangement (**Fig. 3**). The repeat distance, *d*, values (SEM were smaller than 0.02 nm unless indicated otherwise) for all lamellar phases are shown in supplemental Table S2. At 7.5 mol% and 10 mol% ω-*O*-acylCers, LPP with a 12.1 nm repeat period was detected, accompanied by a short periodicity phase (SPP) of $d = 5.3–5.4$ nm (Fig. 3A, black diffractograms, supplemental Table S2). At 20 mol% ω-*O*-acylCers, only LPP was detected ($d = 12.4$ nm; Fig. 3B, black pattern). To challenge the lipid system, the same model with 20 mol% ω-O-acylCers was also prepared at a higher temperature (90°C) and ambient relative humidity. This treatment resulted in the formation of both the LPP ($d = 12.5$ nm) and SPP (5.3 nm; Fig. 3C, black graph). All lipid mixtures also had reflections of separated Chol, consistent with previous results (14, 35, 40).

Next, we replaced all ω-*O*-acylCers with ω-OHCers, thus effectively removing the linoleate moiety from ω-*O*-acylCers simulating the stratum corneum lipids in PNPLA1 deficiency. In the model with ≤10 mol% ω-OHCers, only an SPP with $d = 5.4$ nm was found (Fig. 3A, dark blue diffractogram). The lipid model with 20 mol% ω-OHCer in the Cer fraction assembled into a lamellar phase with 10.8 nm periodicity, the medium lamellar phase, MLP (this assignment was based on 13

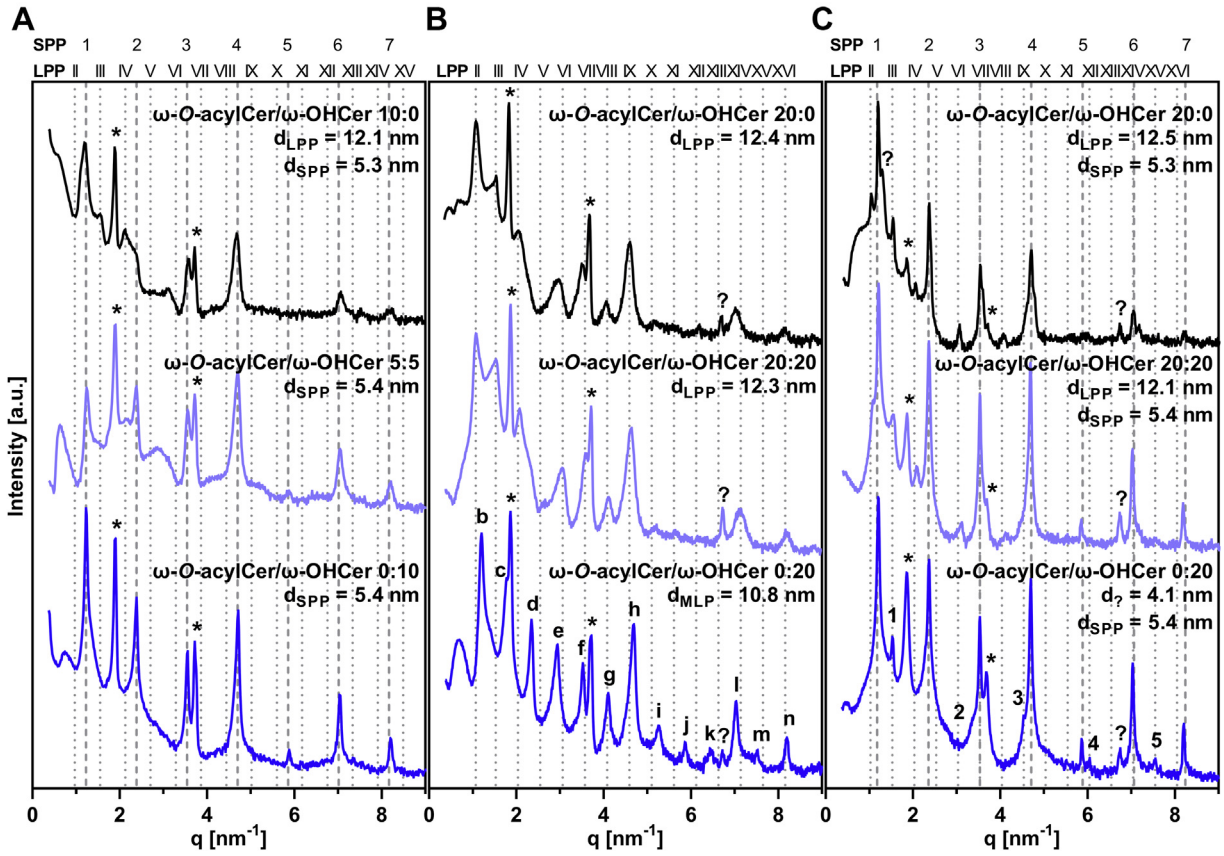

Fig. 3. X-ray diffractograms of the studied lipid films. Models approximating healthy skin condition prepared at 70°C and 100% humidity (A), models with increased ω-*O*-acylCer and ω-OHCer concentration prepared at 70°C and 100% humidity (B), and at 90°C and ambient humidity (C). Individual reflections of the particular lamellar phases are shown using a dotted line (LPP, see figure headings for assignments), dashed line (SPP), or in each diffractogram (letters for MLP, numbers for the unidentified short phase, and asterisks for separated Chol). Representative diffractograms and repeat distance values of all analyzed samples are shown in supplemental Table S2. ω-O-acylCers, omega-O-acylceramides; ω-OHCers, ω-hydroxylated Cers; LPP, long periodicity lamellar phase; SPP, short periodicity phase; MLP, medium lamellar phase; Chol, cholesterol.

reflections, R^2 = 0.9999; Fig. 3B, dark blue graph) (45). Subjecting this lipid model to higher temperature resulted in a loss of the MLP and formation of the SPP (5.4 nm) and an unknown phase with d = 4.1 nm (5 reflections; Fig. 3C, dark blue). The 4.1 nm phase may be rich in ω-OHCer as the calculated length of the 32-carbon atom *N*-acyl chain is 4 nm.

To mimic a partial ω-*O*-acylCer deficiency, two sets of lipid models were constructed containing 5 mol% ω-*O*-acylCers + 5 mol% ω-OHCers (Fig. 3A, light blue graph) and 3.75 mol% ω-*O*-acylCers + 3.75 mol% ω-OHCers (supplemental Table S2). No LPP was detected in either model, confirming that a certain ω-*O*-acylCer concentration threshold (14, 43, 46) is essential for the LPP formation, and no synergy exists between the ω-*O*-acylCers and ω-OHCers.

In another set of models, ω-OHCers (10 and 20 mol% of the Cer fraction) were added to ω-*O*-acylCers (20 mol %) rather than replacing them, roughly mimicking the situation when *Pnpla1*$^{-/-}$ epidermis would be treated with topical ω-*O*-acylCers (Fig. 3B, C, light blue graphs and supplemental Table S2). These lipids had the same lamellar phases as those with 20 mol% ω-*O*-acylCers, indicating that the ω-OHCers did not prevent the LPP formation, given that a sufficient amount of ω-*O*-acylCers was present.

Loss of ω-*O*-acylCer linoleate moiety in the stratum corneum lipid models shifts the orthorhombic-to-hexagonal transition to higher temperatures

The lipid models with 20 mol% ω-*O*-acylCers and 20 mol% ω-OHCers, that is, those forming the LPP and MLP, respectively, were further examined by FTIR (**Fig. 4**). FTIR is a sensitive tool for assessing the lipid chain order and packing. For example, changes in the methylene symmetric stretching bands were found in atopic dermatitis patients compared to healthy volunteers, and such changes correlated with transepidermal water loss (47). Here, mostly well-ordered *all-trans* chains were found in both models at room temperature as indicated by methylene symmetric stretching wavenumbers of 2848.6 cm^{-1}. The lipid chains in both models were tightly packed in orthorhombic subcells as the methylene rocking and scissoring bands were split into doublets (47). Such similarities were rather unexpected given the lack of fluid linoleate in the ω-OHCer model. The major difference between the two models was higher thermal stability of orthorhombic lipid packing in the absence of ω-*O*-acylCer; the vibrational coupling characteristic of orthorhombic packing disappeared at approximately 40°C and at 50°C in the model with ω-*O*-acylCers and ω-OHCers, respectively. With further heating, the lipids in the model with ω-OHCers disordered at slightly higher temperature (by 3°C) than those in the ω-*O*-acylCer model.

The lamellar arrangement of the in vitro lipid models strongly affects their barrier properties; the 10.8 nm lamellar phase, MLP, has similar permeabilities as the LPP

Next, the barrier function of selected lipid films to water loss and two model permeants with various physicochemical properties preferring different permeation routes (48), TH and IND (39, 40, 42), were assessed (**Figs. 5**, S3, and supplemental Table S3). TH was previously used to distinguish the diseased (atopic dermatitis) and healthy permeability barrier (49). The electrical impedance of all tested lipid films was higher than 80 kΩ × cm^2 (data not shown), indicating the absence of macroscopic membrane defects.

The replacement of 10 mol% ω-*O*-acylCers with 10 mol% ω-OHCers increased the water loss by

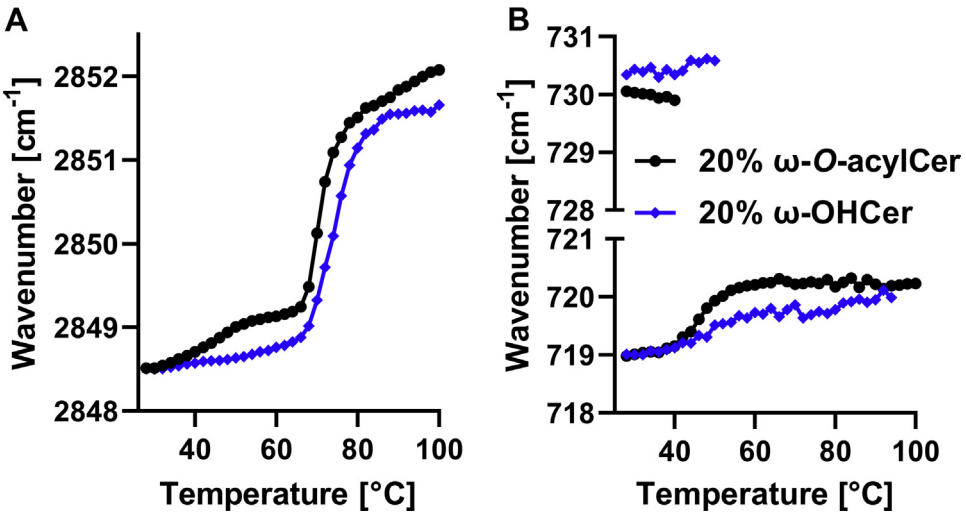

Fig. 4. FTIR spectroscopy of the selected lipid mixtures (20 mol% ω-*O*-acylCers in black and 20 mol% ω-OHCers in blue) shows the phase transitions indicated by the thermal evolution of the methylene symmetric stretching vibration (A) and disappearance of the methylene rocking doublet characteristic of the orthorhombic chain packing (B). FTIR, Fourier-transform infrared spectroscopy; ω-O-acylCers, omega-O-acylceramides; ω-OHCers, ω-hydroxylated Cers.

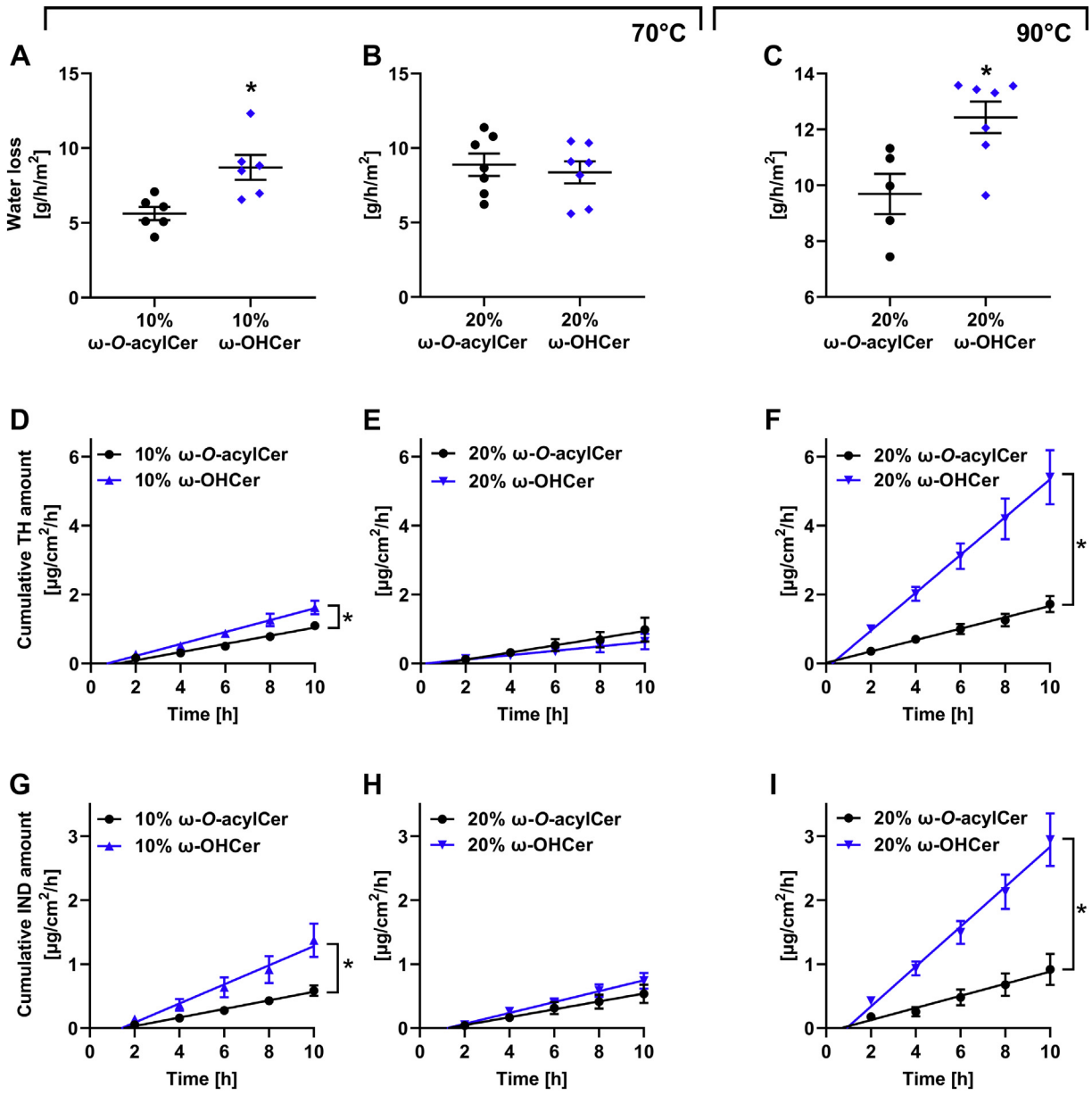

Fig. 5. Permeability properties of the selected lipid mixtures (containing ω-*O*-acylCers in black and ω-OHCers in blue) probed by transmembrane water loss (A–C) and permeation profiles for TH (D, E, F) and IND (G, H, I). Lipid films were annealed at 70°C, 100% humidity (A, B, D, E, G, H) or 90°C, ambient humidity (C, F, I). Values are presented as means ± SEM, n = 5–7. Asterisks indicate statistically significant differences at $P < 0.05$ (*t* test). All water loss and flux values are shown in Supplementary table. ω-O-acylCers, omega-O-acylceramides; ω-OHCers, ω-hydroxylated Cers; TH, theophylline; IND, indomethacin.

approximately 50%, the TH flux by 40%, and the IND flux two-fold (Fig. 5A, D, G), which is consistent with the LPP disappearance. In contrast, no significant differences were found in the models with 20 mol% ω-*O*-acylCers/ω-OHCers, indicating that the MLP formed in the absence of linoleate in the ultralong chain Cer has similar barrier properties to the LPP (Fig. 5B, E, H). The models with a mixture of ω-*O*-acylCer and ω-OHCer had similar permeability properties as models with ω-*O*-acylCers (supplemental Fig. S3). No significant changes in permeability were found between the 10 and 20 mol % ω-*O*-acylCer models, which is consistent with previous studies (14).

Next, we analyzed the permeabilities of the models with the same lipid composition but exposed them to a higher temperature during assembly (Fig. 5C, F, I). The barrier properties of the samples containing 20 mol% ω-*O*-acylCers (either without or with ω-OHCers) prepared at 90°C slightly decreased compared to the model with the same lipid composition annealed at 70°C, likely reflecting the SPP and LPP coexistence in the former. In sharp contrast, the ω-OHCer models prepared at 90°C, had eight- and three-fold higher permeabilities to TH and IND, respectively, than those assembled at 70°C. The water barrier was relatively less sensitive to such change.

DISCUSSION

The linoleate moiety of ω-*O*-acylCers is essential for binding to corneocyte proteins and forming the CLE (17–19). Our results revealed that apart from CLE formation, the linoleate chain in ω-*O*-acylCers is essential for assembling the barrier lipid precursors in the lamellar bodies and the free stratum corneum lipids into the LPP. In the absence of ω-*O*-acylCer, single bands rather than paired bands were observed in the lamellar bodies of *Pnpla1*$^{-/-}$ mice, suggesting that the ω-*O*-acylCer linoleate tails are present in the electron-dense layer in the center of the paired lamella in wt mice resembling lipid droplet lens. In *Pnpla1*$^{-/-}$ mice, these single bands were transferred from the lamellar bodies to the intercellular spaces of the stratum corneum. This behavior is consistent with the proposed hierarchical two-step assembly of healthy skin barrier lipids; the lipid precursors assemble at the molecular level in the lamellar bodies, and the final stratum corneum lamellae develop from these prefabricated nano-sized lipid stacks (50). Putatively, postsecretory lipid processing destabilizes the paired bilayer-like arrangement, and this stress may be relieved by flipping the sphingoid base chain to an extended Cer conformation (51–53). Thus, the broad lucent bands in the triplets could be enriched in rigid and tightly packed acyl chains, while the narrow lucent band might be rich in the sphingoid base chains and Chol.

To gain further insight into the behavior of stratum corneum lipids in *Pnpla1*$^{-/-}$ mice, we attempted to reproduce some of the prominent features of the lipid lamellae in the absence of the ω-*O*-acylCer linoleate tails using in vitro lipid models. The models in which ω-*O*-acylCers were replaced by ω-OHCers lost the LPP architecture, consistent with the TEM images of *Pnpla1*$^{-/-}$ mice. At 10 mol% ω-OHCer concentration, the lipids formed the SPP and their weaker barrier agreed with the LPP loss (14). Lipids in the 20 mol% ω-OHCer model arranged themselves in a phase with 10.8 nm periodicity, the MLP, with similar barrier properties to the LPP in the 20 mol% ω-*O*-acylCer model. A conceivable explanation of the MLP structure is that it comprises two SPP units (if we assume that SPP is asymmetrical) or SPP-like units (45). Such a unit would very likely contain Cers in the extended (splayed-chain) conformation with acyl chains pointing to opposite directions (51–53). Arranging such two units face-to-face would lead to a doubled periodicity, as observed for the MLP (45, 54). Lipid arrangement with approximately 10 nm periodicity was observed in the stratum corneum of *Pnpla1*$^{-/-}$ mice, although without detailed data about the inner structures of these phases no link can be drawn to the MLP found in the lipid model.

Notably, previous in vitro lipid models showed that LPP is assembled when linoleate in ω-*O*-acylCer is replaced by oleate but not stearate, albeit the SPP/LPP ratio increased upon replacement of linoleate by oleate (55). Thus, the ultralong *N*-acyl chain in ω-*O*-acylCer, which is approximately 4 nm long and therefore can span a bilayer, does not per se induce the LPP assembly, which explicitly requires an unsaturated ω-*O*-acyl moiety.

The loss of the linoleate moiety in our model shifted the orthorhombic-hexagonal lipid transition, which involves loosening the tightly packed lipid chains, to higher temperatures. This higher stability of orthorhombic packing may be beneficial in reducing water permeability but shifting the transition out of the physiological range of 35–40°C (56) may have as yet unknown implications on epidermal homeostasis.

To study the robustness of the LPP and MLP arrangements, the lipid models with 20 mol% ω-*O*-acylCer/ω-OHCers were assembled at 90°C. The LPP was still present in the ω-*O*-acylCer model (similar to isolated human stratum corneum lipids (57)), but in the ω-OHCer model, the MLP dissolved into the SPP and a 4.1 nm phase, rendering lipid films 3 and 8-fold more permeable.

The observed lamellar rearrangement was caused by the absence of ω-*O*-acylCers and not the presence of ω-OHCers, since the lipid models combining ω-*O*-acylCers with ω-OHCers retained the LPP when they had sufficient ω-*O*-acylCers. Thus, the free hydroxyl group of ω-OHCers does not have any significant adverse effects on the lipid organization and permeability barrier function of the stratum corneum, and replacement of the missing ω-*O*-acylCers appears to be a viable therapeutic strategy in ichthyosis patients with PNPLA1 deficiency (provided that the ω-*O*-acylCers can be delivered to deeper stratum corneum in sufficient quantities). The potential of such lipid replacement was shown by applying epidermal lipid extracts from WT mice onto the skin of *Pnpla1* $^{-/-}$ mice, which resulted in the synthesis of protein-bound ω-OHCers, indicating the rebuilding of the CLE in PNPLA1-deficient skin (31). Mauldin *et al.* treated NIPAL4-deficient dogs (another lipid-synthetic ARCI that converges on the CLE) with ω-*O*-acylCers, rescuing both the CLE and also the underlying protein corneocyte envelope (although the clinical phenotype only partially improved due to an accumulation of proximal toxic metabolites) (58). In addition, ω-*O*-acylCer EOS partially reversed the expression of *Flg*, *Ppard*, and *Hbegf* in *Pnpla1*$^{-/-}$ keratinocytes (32).

Considering the relatively small effects of the lipid organization on water loss in our lipid models, it appears that the lack of the LPP only partly contributes to the diminished water permeability barrier in *Pnpla1*$^{-/-}$ mice. These mice show an approximately three- to four-fold increased water loss than their wt littermates (30, 31). Although direct comparison of our lipid models with in vivo data is not possible since the diminished levels of filaggrin and loricrin as well as hyperactivation of PPARδ in *Pnpla1*$^{-/-}$ mice may also

contribute to the altered barrier function (32), the lack of the CLE may be a conceivable explanation for the impaired water permeability barrier in *Pnpla1*$^{-/-}$ mice. The absence of this covalent hydrophobic cell coat likely renders the corneocytes leakier to hydrophilic substances and leaves the hydrophobic lipids without their tether to the hydrophilic cell surface, thus creating a permeable boundary or making the lipid arrangement weaker to external stressors.

CONCLUSIONS

Our results show that ω-*O*-acylCers are essential for lamellae pairing in lamellar bodies and stratum corneum lipid assembly into the LPP, apart from its role in CLE formation. ω-OHCers lack the linoleate moiety and cannot substitute for ω-*O*-acylCers, although at favorable conditions, they form almost 11 nm lamellae, the MLP, with permeability characteristics similar to the LPP. Unlike the LPP, the MLP is sensitive to conditions during assembly and may dissolve into two phases with diminished barrier properties. The lipid models combining ω-OHCers with ω-*O*-acylCers suggest that ω-OHCers do not perturb the lipid organization per se and that ω-*O*-acylCer replacement may be a viable therapeutic option in patients with PNPLA1 deficiency.

Data availability

Additional data are available in the Supplementary information file.

Supplemental data

This article contains supplemental data (4).

Acknowledgments

We thank Dr Susanne Grond, Mrs. Iva Vencovská, and Dr Jaroslav Maixner for their help with the *Pnpla1*$^{+/+}$ and *Pnpla1*$^{-/-}$ mice, FTIR, and XRD experiments, respectively. This work was supported by the Czech Science Foundation, Czechia (19–09135J and 22–20839K), Charles University, Czechia (GAUK 1194119 and SVV 260 547), and by the project EFSA-CDN (CZ.02.1.01/0.0/0.0/16_019/0000841) cofunded by the European Union, European Union.

Author contributions

L. O., J. M. M., F. P. W. R., and K. V. methodology; L. O., J. M. M., F. P. W. R., and K. V. validation; L. O., J. M. M., V. O., and L. S. investigation; L. O., J. M. M., V. O., and L. S. data curation; L. O. and K. V. writing–original draft; L. O., J. M. M., V. O., L. S., F. P. W. R., and K. V. writing–review and editing; L. O., J. M. M., and K. V. visualization; K. V. conceptualization; K. V. supervision; K. V. funding acquisition.

Author ORCIDs

Lukáš Opálka https://orcid.org/0000-0003-1379-1406
Jason M. Meyer https://orcid.org/0000-0003-1327-3510
Veronika Ondrejčeková https://orcid.org/0000-0002-5402-3027
Franz P.W. Radner https://orcid.org/0000-0003-3466-0181
Kateřina Vávrová https://orcid.org/0000-0002-8502-4372

Conflict of interest

The authors declare that they have no conflicts of interest with the contents of this article.

Abbreviations

Cers, ceramides; Chol, cholesterol; CholS, cholesteryl sulfat; CLE, corneocyte lipid envelope; FFAs, free fatty acids; FTIR, Fourier-transform infrared spectroscopy; IND, indomethacin; LPP, long periodicity lamellar phase; MLP, medium lamellar phase; SPP, short periodicity phase; TH, theophylline; XRD, X-ray diffraction; ω-O-acylCers, omega-O-acylceramides; ω-OHCers, ω-hydroxylated Cers.

Manuscript received March 4, 2022, and in revised from May 3, 2022, .accepted May 9, 2022 Published, JLR Papers in Press, May 12, 2022, https://doi.org/10.1016/j.jlr.2022.100226

REFERENCES

1. Madison, K. C. (2003) Barrier function of the skin: "La Raison d'Etre" of the epidermis. *J. Invest. Dermatol.* **121**, 231–241
2. Elias, P. M. (1991) Epidermal barrier function: intercellular lamellar lipid structures, origin, composition and metabolism. *J. Control Release.* **15**, 199–208
3. Masukawa, Y., Narita, H., Sato, H., Naoe, A., Kondo, N., Sugai, Y., *et al.* (2009) Comprehensive quantification of ceramide species in human stratum corneum. *J. Lipid Res.* **50**, 1708–1719
4. Motta, S., Monti, M., Sesana, S., Caputo, R., Carelli, S., and Ghidoni, R. (1993) Ceramide composition of the psoriatic scale. *Biochim. Biophys. Acta.* **1182**, 147–151
5. van Smeden, J., Boiten, W. A., Hankemeier, T., Rissmann, R., Bouwstra, J. A., and Vreeken, R. J. (2014) Combined LC/MS-platform for analysis of all major stratum corneum lipids, and the profiling of skin substitutes. *BBA-Mol. Cell Biol. L.* **1841**, 70–79
6. t'Kindt, R., Jorge, L., Dumont, E., Couturon, P., David, F., Sandra, P., *et al.* (2012) Profiling and characterizing skin ceramides using reversed-phase liquid chromatography-quadrupole time-of-flight mass spectrometry. *Anal. Chem.* **84**, 403–411
7. Wertz, P. W., and Downing, D. T. (1983) Ceramides of pig epidermis: structure determination. *J. Lipid Res.* **24**, 759–765
8. Bowser, P. A., Nugteren, D., White, R. J., Houtsmuller, U., and Prottey, C. (1985) Identification, isolation and characterization of epidermal lipids containing linoleic acid. *Biochim. Biophys. Acta.* **834**, 419–428
9. Kihara, A. (2016) Synthesis and degradation pathways, functions, and pathology of ceramides and epidermal acylceramides. *Prog. Lipid Res.* **63**, 50–69
10. Ishikawa, J., Narita, H., Kondo, N., Hotta, M., Takagi, Y., Masukawa, Y., *et al.* (2010) Changes in the ceramide profile of Atopic Dermatitis patients. *J. Invest. Dermatol.* **130**, 2511–2514
11. Janssens, M., van Smeden, J., Gooris, G. S., Bras, W., Portale, G., Caspers, P. J., *et al.* (2011) Lamellar lipid organization and ceramide composition in the stratum corneum of patients with atopic eczema. *J. Invest. Dermatol.* **131**, 2136–2138
12. Bouwstra, J. A., Cheng, K., Gooris, G., Weerheim, A., and Ponec, M. (1996) The role of ceramides 1 and 2 in the stratum corneum lipid organisation. *Bba-lipid. Lipid Met.* **1300**, 177–186
13. Bouwstra, J. A., Gooris, G. S., Dubbelaar, F. E. R., Weerheim, A. M., Ijzerman, A. P., and Ponec, M. (1998) Role of ceramide 1 in the molecular organization of the stratum corneum lipids. *J. Lipid Res.* **39**, 186–196
14. Opálka, L., Kováčik, A., Pullmannová, P., Maixner, J., and Vávrová, K. (2020) Effects of omega-O-acylceramide structures and concentrations in healthy and diseased skin barrier lipid membrane models. *J. Lipid Res.* **61**, 219–228

15. Pham, Q. D., Mojumdar, E. H., Gooris, G. S., Bouwstra, J. A., Sparr, E., and Topgaard, D. (2018) Solid and fluid segments within the same molecule of stratum corneum ceramide lipid. *Q. Rev. Biophys.* **51**, e7
16. Ongpipattanakul, B., Francoeur, M. L., and Potts, R. O. (1994) Polymorphism in stratum corneum lipids. *BBA-Biomem.* **1190**, 115–122
17. Takeichi, T., Hirabayashi, T., Miyasaka, Y., Kawamoto, A., Okuno, Y., Taguchi, S., *et al.* (2020) SDR9C7 catalyzes critical dehydrogenation of acylceramides for skin barrier formation. *J. Clin. Invest.* **130**, 890–903
18. Wertz, P. W., Madison, K. C., and Downing, D. T. (1989) Covalently bound lipids of human stratum corneum. *J. Invest. Dermatol.* **92**, 109–111
19. Akiyama, M. (2017) Corneocyte lipid envelope (CLE), the key structure for skin barrier function and ichthyosis pathogenesis. *J. Dermatol. Sci.* **88**, 3–9
20. Crumrine, D., Khnykin, D., Krieg, P., Man, M-Q., Celli, A., Mauro, T. M., *et al.* (2019) Mutations in recessive congenital ichthyoses illuminate the origin and functions of the corneocyte lipid envelope. *J. Invest. Dermatol.* **139**, 760–768
21. Janssens, M., van Smeden, J., Gooris, G. S., Bras, W., Portale, G., Caspers, P. J., *et al.* (2012) Increase in short-chain ceramides correlates with an altered lipid organization and decreased barrier function in atopic eczema patients. *J. Lipid Res.* **53**, 2755–2766
22. Jennemann, R., Rabionet, M., Gorgas, K., Epstein, S., Dalpke, A., Rothermel, U., *et al.* (2012) Loss of ceramide synthase 3 causes lethal skin barrier disruption. *Hum. Mol. Genet.* **21**, 586–608
23. van Smeden, J., Janssens, M., Gooris, G. S., and Bouwstra, J. A. (2014) The important role of stratum corneum lipids for the cutaneous barrier function. *BBA-Mol. Cell Biol. L.* **1841**, 295–313
24. Macheleidt, O., Kaiser, H. W., and Sandhoff, K. (2002) Deficiency of epidermal protein-bound omega-hydroxyceramides in atopic dermatitis. *J. Invest. Dermatol.* **119**, 166–173
25. Jungersted, J., Scheer, H., Mempel, M., Baurecht, H., Cifuentes, L., Høgh, J., *et al.* (2010) Stratum corneum lipids, skin barrier function and filaggrin mutations in patients with atopic eczema. *Allergy.* **65**, 911–918
26. Paige, D., Morse-Fisher, N., and Harper, J. (1994) Quantification of stratum corneum ceramides and lipid envelope ceramides in the hereditary ichthyoses. *Br. J. Dermatol.* **131**, 23–27
27. Oji, V., Tadini, G., Akiyama, M., Bardon, C. B., Bodemer, C., Bourrat, E., *et al.* (2010) Revised nomenclature and classification of inherited ichthyoses: results of the first ichthyosis consensus conference in soreze 2009. *J. Am. Acad. Dermatol.* **63**, 607–641
28. Takeichi, T., and Akiyama, M. (2016) Inherited ichthyosis: non-syndromic forms. *J. Dermatol.* **43**, 242–251
29. Ohno, Y., Kamiyama, N., Nakamichi, S., and Kihara, A. (2017) PNPLA1 is a transacylase essential for the generation of the skin barrier lipid ω-O-acylceramide. *Nat. Commun.* **8**, 14610
30. Pichery, M., Huchenq, A., Sandhoff, R., Severino-Freire, M., Zaafouri, S., Opalka, L., *et al.* (2017) PNPLA1 defects in patients with autosomal recessive congenital ichthyosis and KO mice sustain PNPLA1 irreplaceable function in epidermal omega-O-acylceramide synthesis and skin permeability barrier. *Hum. Mol. Genet.* **26**, 1787–1800
31. Grond, S., Eichmann, T. O., Dubrac, S., Kolb, D., Schmuth, M., Fischer, J., *et al.* (2017) PNPLA1 deficiency in mice and humans leads to a defect in the synthesis of omega-O-acylceramides. *J. J. Invest. Dermatol.* **137**, 394–402
32. Hirabayashi, T., Anjo, T., Kaneko, A., Senoo, Y., Shibata, A., Takama, H., *et al.* (2017) PNPLA1 has a crucial role in skin barrier function by directing acylceramide biosynthesis. *Nat. Commun.* **8**, 1–13
33. Grall, A., Guaguère, E., Planchais, S., Grond, S., Bourrat, E., Hausser, I., *et al.* (2012) PNPLA1 mutations cause autosomal recessive congenital ichthyosis in golden retriever dogs and humans. *Nat. Genet.* **44**, 140
34. Opálka, L., Kováčik, A., Sochorová, M., Roh, J., Kuneš, J., Lenčo, J., *et al.* (2015) Scalable synthesis of human ultralong chain ceramides. *Org. Lett.* **17**, 5456–5459
35. Kováčik, A., Vogel, A., Adler, J., Pullmannová, P., Vávrová, K., and Huster, D. (2018) Probing the role of ceramide hydroxylation in skin barrier lipid models by 2 H solid-state NMR spectroscopy and X-ray powder diffraction. *BBA-Biomem.* **1860**, 1162–1170
36. Meyer, J. M., Crumrine, D., Schneider, H., Dick, A., Schmuth, M., Gruber, R., *et al.* (2021) Unbound corneocyte lipid envelopes in 12R-lipoxygenase deficiency support a specific role in lipid-protein cross-linking. *Am. J. Pathol.* **191**, 921–929
37. Groen, D., Gooris, G. S., and Bouwstra, J. A. (2010) Model membranes prepared with ceramide EOS, cholesterol and free fatty acids form a unique lamellar phase. *Langmuir.* **26**, 4168–4175
38. Wertz, P. W., Schwartzendruber, D. C., Madison, K. C., and Downing, D. T. (1987) Composition and morphology of epidermal cyst lipids. *J. Invest. Dermatol.* **89**, 419–425
39. Školová, B., Janůšová, B., Zbytovská, J., Gooris, G., Bouwstra, J., Slepička, P., *et al.* (2013) Ceramides in the skin lipid membranes: length matters. *Langmuir.* **29**, 15624–15633
40. Pullmannová, P., Staňková, K., Pospíšilová, M., Školová, B., Zbytovská, J., and Vávrová, K. (2014) Effects of sphingomyelin/ceramide ratio on the permeability and microstructure of model stratum corneum lipid membranes. *BBA-Biomem.* **1838**, 2115–2126
41. Pullmannová, P., Pavlíková, L., Kováčik, A., Sochorová, M., Školová, B., Slepička, P., *et al.* (2017) Permeability and microstructure of model stratum corneum lipid membranes containing ceramides with long (C16) and very long (C24) acyl chains. *Biophys. Chem.* **224**, 20–31
42. Kovacik, A., Pullmannová, P., Maixner, J., and Vavrova, K. (2018) Effects of ceramide and dihydroceramide stereochemistry at C-3 on the phase behavior and permeability of skin lipid membranes. *Langmuir.* **34**, 521–529
43. Opálka, L., Kováčik, A., Maixner, J., and Vávrová, K. (2016) Omega-O-acylceramides in skin lipid membranes: effects of concentration, sphingoid base, and model complexity on microstructure and permeability. *Langmuir.* **32**, 12894–12904
44. Hou, S. Y. E., Mitra, A. K., White, S. H., Menon, G. K., Ghadially, R., and Elias, P. M. (1991) Membrane structures in normal and essential fatty acid-deficient stratum corneum: characterization by ruthenium tetroxide staining and x-ray diffraction. *J. Invest. Dermatol.* **96**, 215–223
45. Pullmannova, P., Ermakova, E., Kovacik, A., Opalka, L., Maixner, J., Zbytovska, J., *et al.* (2019) long and very long lamellar phases in model Stratum Corneum lipid membranes. *J. Lipid Res.* **60**, 963–971
46. de Jager, M., Gooris, G., Ponec, M., and Bouwstra, J. (2004) Acylceramide head group architecture affects lipid organization in synthetic ceramide mixtures. *J. Invest. Dermatol.* **123**, 911–916
47. Damien, F., and Boncheva, M. (2010) The extent of orthorhombic lipid phases in the stratum corneum determines the barrier efficiency of human skin in vivo. *J. Invest. Dermatol.* **130**, 611–614
48. Mitragotri, S. (2003) Modeling skin permeability to hydrophilic and hydrophobic solutes based on four permeation pathways. *J. Control Release.* **86**, 69–92
49. Yoshiike, T., Aikawa, Y., Sindhvananda, J., Suto, H., Nishimura, K., Kawamoto, T., *et al.* (1993) Skin barrier defect in atopic dermatitis: increased permeability of the stratum corneum using dimethyl sulfoxide and theophylline. *J. Dermatol. Sci.* **5**, 92–96
50. Boncheva, M. (2014) The physical chemistry of the stratum corneum lipids. *Int. J. Cosmet. Sci.* **36**, 505–515
51. Engberg, O., Kováčik, A., Pullmannová, P., Juhaščik, M., Opálka, L., Huster, D., *et al.* (2020) The sphingosine and acyl chains of ceramide [NS] show very different structure and dynamics that challenge our understanding of the skin barrier. *Angew. Chem. Int. Ed.* **59**, 17383–17387
52. Iwai, I., Han, H., den Hollander, L., Svensson, S., Öfverstedt, L-G., Anwar, J., *et al.* (2012) The human skin barrier is organized as stacked bilayers of fully extended ceramides with cholesterol molecules associated with the ceramide sphingoid moiety. *J. Invest. Dermatol.* **132**, 2215–2225
53. Školová, B., Hudská, K., Pullmannová, P., Kováčik, A., Palát, K., Roh, J., *et al.* (2014) Different phase behavior and packing of ceramides with long (C16) and very long (C24) acyls in model membranes: infrared spectroscopy using deuterated lipids. *J. Phys. Chem. B.* **118**, 10460–10470
54. Kováčik, A., Opálka, L., Šilarová, M., Roh, J., and Vávrová, K. (2016) Synthesis of 6-hydroxyceramide using ruthenium-catalyzed hydrosilylation–protodesilylation. Unexpected formation of a long periodicity lamellar phase in skin lipid membranes. *RSC Adv.* **6**, 73343–73350

55. Bouwstra, J. A., Gooris, G. S., Dubbelaar, F. E., and Ponec, M. (2002) Phase behavior of stratum corneum lipid mixtures based on human ceramides: the role of natural and synthetic ceramide 1. *J. Invest. Dermatol.* **118**, 606–617
56. Bouwstra, J., Gooris, G., Salomons-de Vries, M., Van der Spek, J., and Bras, W. (1992) Structure of human stratum corneum as a function of temperature and hydration: a wide-angle X-ray diffraction study. *Int. J. Pharm.* **84**, 205–216
57. Sagrafena, I., Paraskevopoulos, G., Pullmannová, P., Opálka, L., Nováčková, A., Lourantou, O., *et al.* (2022) Assembly of human stratum corneum lipids in vitro: fluidity matters. *J. Invest. Dermatol.* https://doi.org/10.1016/j.jid.2021.12.008
58. Mauldin, E. A., Crumrine, D., Casal, M. L., Jeong, S., Opálka, L., Vavrova, K., *et al.* (2018) Cellular and metabolic basis for the ichthyotic phenotype in NIPAL4 (Ichthyin)–deficient canines. *Am. J. Pathol.* **188**, 1419–1429